Uncertainty and Disturbance Estimator-Based Global Trajectory Tracking Control for a Quadrotor

Qi Lu, *Member, IEEE*, Beibei Ren, *Senior Member, IEEE*, and Siva Parameswaran

***Abstract*—This article presents an uncertainty and disturbance estimator (UDE) based global trajectory tracking control strategy for a quadrotor. The main contribution of this article is the fusion of the UDE technique with the unit quaternion to achieve the robust global full degrees of freedom trajectory tracking control with experimental demonstrations. The novelty of this article lies in the development of the UDE-based global tracking technique to the overall system (attitude and position) with a quaternion-based nonlinear reference model. The UDE-based attitude and position controllers are derived from the unit quaternion-based quadrotor dynamics with a cascade control structure to deal with underactuation, model uncertainties, and external disturbances. The attitude controllers that are developed with the backstepping techniques avoid the rotation matrix calculation and the unwinding problem. The position controllers are derived using the thrust-vectoring approach. A nonlinear unit quaternion-based reference model is developed to achieve the time-scale separation for the cascade control loops. The stability analysis of the closed-loop system is conducted with the Lyapunov method. Extensive flight experiments are conducted to demonstrate the global singularity-free tracking property and the superior robustness of the proposed controller.**

***Index Terms*—Quadrotor, robust control, uncertainty and disturbance estimator (UDE), unit quaternion.**

I. Introduction

THE rapid innovation in sensing and control technologies in recent years enabled the successful applications of quadrotors to various applications including aerial filming, government law enforcement, and package delivery [1], [2]. Among various flying platforms, the quadrotor possesses the merits of mechanical simplicity and high maneuverability, which make it suitable to accomplish flight missions in limited space and cluttered environment [1], [3]. The level of quadrotor's maneuverability is closely related to the flight control algorithm, which is greatly limited by conventional attitude representation methods, such as Euler angle [4]. For some scenarios, where the quadrotor is required to perch on inclined surfaces in order to work as a radio relay [5] or to continuously rotate to fly in the case of rotor failure [6], flight control algorithms capable of large angle maneuvers become necessity.

In order to fully explore the potential of quadrotor's maneuverability, there are several challenges that need to be tackled. First, the quadrotor is a naturally unstable system with inherently nonlinear underactuated coupled dynamics [1], which creates difficulties for the control algorithm development. Second, the quadrotor model used for controller development is usually inaccurate or incomprehensive. The model mismatch that may be caused by payload change or the time-varying model uncertainty, which is caused by battery voltage dropping can degrade the tracking performance. Third, though the small size and lightweight features of a quadrotor bring the benefit of agility [7], the low inertia also renders the quadrotor susceptible to external disturbances, such as wind. Fourth, the attitude dynamics evolves on a nonlinear manifold, which is called the special orthogonal group, $SO(3)$ [8]. To achieve the global singularity-free attitude representation, nonlinear attitude representation methods, such as rotation matrix and unit quaternion are needed [9]. Fifth, the onboard hardware is usually based on embedded processors with low memory and processing power [10]. The limited computational resources constrain the implementation of computationally demanding flight control algorithms.

Over the past decades, in order to handle the abovementioned challenges, various flight control algorithms have been proposed. Based on the commonly used attitude representation methods, the quadrotor control design methods can be roughly grouped into three categories. The first category utilizes Euler angles for attitude representation in flight control design, which is simple and easy to implement since the three Euler angles can be directly mapped to the three attitude control inputs. Therefore, the Euler angle-based attitude representation method has been widely adopted in different control algorithms, such as the commonly used PID control [11], the adaptive controllers developed with immersion and invariance technique [12], and the robust control strategies derived using sliding mode technique [13], robust compensating technique [14], active disturbance rejection control [15], differential flatness property [16] and uncertainty

Manuscript received October 15, 2019; revised January 23, 2020; accepted February 19, 2020. Date of publication March 6, 2020; date of current version June 15, 2020. Recommended by Technical Editor M. Indri. *(Corresponding author: Beibei Ren.)*

Qi Lu is with the Department of Mechanical Engineering, Sichuan University-Pittsburgh Institute, Sichuan University, Chengdu, Sichuan 610207, China (e-mail: qi.lu@scu.edu.cn).

Beibei Ren and Siva Parameswaran are with the Department of Mechanical Engineering, Texas Tech University, Lubbock, TX 79409 USA (e-mail: beibei.ren@ttu.edu; siva.parameswaran@ttu.edu).

Color versions of one or more of the figures in this article are available online at http://ieeexplore.ieee.org.

Digital Object Identifier 10.1109/TMECH.2020.2978529

and disturbance estimator (UDE) based robust control [17]–[19]. However, there exist mathematical singularities, called "gimbal lock" [20], in the Euler angle attitude representation method. Such singularities lead to the failure of the developed control strategies for achieving large angle maneuvers [9]. Therefore, it motivates the second group of researchers to derive geometric controllers directly from the nonlinear manifold SO(3) [8], [9], [21]–[23], which naturally overcomes the singularities associated with minimal attitude representations. In [9] and [22], the geometric controllers based on exponential coordinates have been developed. However, the external disturbances and model uncertainties were not considered in the controller derivation process in [22]. An intrinsic PID controller has been proposed in [23]. The integral action was introduced to handle the bounded parametric uncertainties and disturbances. The adaptive geometric controller development has been investigated in [8] and [21]. The adaptive control laws were introduced to handle uncertainties and disturbances. However, the bound information of the disturbance term was needed in [8]. The third category includes the unit quaternion-based approaches, where the unit quaternion achieves minimal global nonsingular attitude representation with four parameters, bringing the benefits of the computational efficiency compared to matrix manipulations. In [24], the attitude stabilization of a quadrotor was tackled by a PD^2 controller in terms of the unit quaternion. The compensation of Coriolis and gyroscopic torques were achieved with feedforward terms. Due to the mechanical limitation of the conventional quadrotor, where only the upward lift can be generated, a nonlinear quaternion-based control algorithm was proposed for a variable pitch quadrotor in [25] to achieve the agile flight. Nevertheless, the aforementioned unit quaternion-based controllers were developed without considering the effects of model uncertainties and external disturbances. The unit quaternion-based attitude controllers were developed in [26] and [27] with robust compensators to deal with the model uncertainties and external disturbances. The combination of the unit quaternion and the disturbance observer (DOB) has been investigated in [28] with the aggressive maneuver demonstrated. The motor dynamics was taken into account to increase the observer bandwidth. However, only the attitude control strategies of a quadrotor were considered in [26]–[28]. Although the DOB-based control [28], the robust compensator-based control [29], and the UDE-based control [30] are similar in the sense that they adopt filters to estimate the uncertainties and disturbances, they are different control strategies. The DOB-based control and the robust compensator-based control involve taking the inverse of the nominal plant model in the frequency-domain, whereas the UDE-based control does not. Therefore, the UDE-based control is applicable to a wider class of systems [31]. Furthermore, the UDE-based control evolved from the time-delay control (TDC) [32]. The TDC consists of a reference model, an error feedback term, and an estimation of the uncertainty and disturbance using time delay. The UDE-based control [30] employs a filter instead of a delay term to observe the uncertainty and disturbance with the benefits of no delay in the system, no oscillations in the control signal, and no need of measuring the state vector derivatives. A full DOFs unit quaternion-based hybrid control strategy was developed in [1] with the robustness to parametric uncertainties and external disturbances. However, the attitude recovery and autonomous hover maneuver from large undesirable initial angles (beyond $\pm \frac{\pi}{2}$), which are generated by hand tossing, using onboard sensing, and computation in a GPS-denied environment, still remains as a challenging task.

The novelties of this article lie in 1) the development of the UDE-based full degrees-of-freedom (DOFs) quadrotor control system with the unit quaternion formulation to overcome the Euler angle singularity and the computational constraints for onboard implementation; and 2) the introduction of a nonlinear reference model, which observes the quaternion differential kinematics to achieve the time-scale separation between the cascade control loops. The ambiguity problem of the unit quaternion attitude representation is solved with the introduction of a virtual controller. The UDE-based robust control strategies are adopted to handle system coupling, model uncertainties, and external disturbances. The performance of the developed control strategies is demonstrated through the implementation on a quadrotor to achieve large angle maneuvers with only onboard sensing and computation. The UDE-based control algorithm, which is proposed in [30], has drawn considerable amount of attention in both theoretical [31], [33] and application [17]–[19] perspectives due to the advantages of clear structure and easy tuning. The remarkable performance of UDE-based controllers is demonstrated on quadrotors for attitude control [17], trajectory tracking control [18], and landing control [19]. The contributions of this article are highlighted as follows.

1) The UDE-based attitude controllers have been developed with the introduction of the unit quaternion to achieve the global nonsingular attitude tracking while concurrently defeating the effects of system coupling, model uncertainties, and external disturbances. Inspired by [33], the backstepping technique is applied to deal with the highly nonlinear quaternion error dynamics. The developed controller is computationally efficient since it avoids the calculation of the rotation matrix, which has been adopted in [1] and [34]. The unwinding problem, which is caused by the unit quaternion ambiguity is handled by the proposed virtual controller. Furthermore, the detailed stability analysis of the closed-loop system is conducted.
2) With the cascade control architecture and the thrust-vectoring approach, the UDE-based position controllers have been derived to achieve the accurate trajectory tracking and to solve the underactuation problem. The total thrust and desired orientation are calculated from the commanded accelerations without any linearization or approximation. The proposed approach also avoids the singularity problem, which can be caused by the construction of inverse trigonometric function operators [11], [12]. Furthermore, a nonlinear reference model is introduced between position and attitude control loops to achieve the time-scale separation.
3) The proposed approach is validated with quadrotor flight experiments using only onboard sensing and computation in a GPS-denied environment. The performance of the developed unit quaternion-based controllers are demonstrated with the attitude recovery and autonomous hover from the undesirable large initial angle, i.e.,

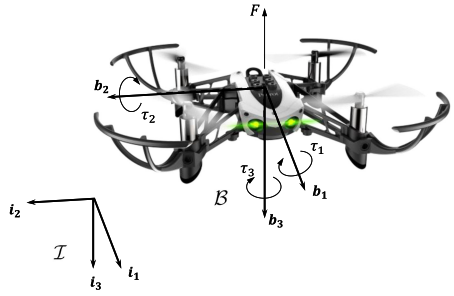

Fig. 1. Quadrotor coordinate systems with inertia reference frame $\mathcal{I}$ and body-fixed frame $\mathcal{B}$.

-117.252 degrees, which has passed the mathematical and mechanical singularity, i.e., $-90°$, the complex trajectory tracking in the presence of wind disturbance, and the comparison with the newly developed unit quaternion-based robust controller [1] considering both model uncertainty and disturbance. The experimental results demonstrate the superior robustness of the proposed controller for handling model uncertainties and external disturbances over [1]. Compared with our previously published works [18], [19], which were developed based on Euler angle attitude representation, the capabilities and the operation ranges of the proposed controllers are further improved with the demonstration of more challenging flight maneuvers.

The rest of this article is organized as follows. Section II presents the preliminaries about the unit quaternion, the unit quaternion-based quadrotor system modeling, and the problem formulation. Section III discusses the developments of the unit quaternion-based robust control design and the nonlinear reference model. Section IV shows the proof of the closed-loop system stability. The effectiveness of the proposed approach is demonstrated through flight experiments in Section V. Section VI concludes this article.

II. System Modeling and Problem Formulation

A. Preliminaries

The coordinate systems used for developing the quadrotor dynamic models are shown in Fig. 1.

Let $\mathcal{I} = \{\boldsymbol{i_1}\ \boldsymbol{i_2}\ \boldsymbol{i_3}\}$ represent the right-hand inertia reference frame with $\boldsymbol{i_1}$, $\boldsymbol{i_2}$, and $\boldsymbol{i_3}$ being three mutually orthogonal unit direction vectors, where $\boldsymbol{i_3}$ is pointing downward. The body-fixed frame is denoted by $\mathcal{B} = \{\boldsymbol{b_1}\ \boldsymbol{b_2}\ \boldsymbol{b_3}\}$ with the origin attached to the center of gravity of the quadrotor, where $\boldsymbol{b_1}$, $\boldsymbol{b_2}$, and $\boldsymbol{b_3}$ are three unit vectors. According to the Euler's rotation theorem, every rotation of a rigid body in three-dimensional space is equivalent to a single rotation about some fixed axis, which is described by a unit vector $\mathbf{r}$, and a rotation angle β. Therefore, the unit quaternion that represents the quadrotor attitude in $\mathcal{I}$ could be defined as [35]

$$\mathbf{q} = \begin{bmatrix} q_0 & q_1 & q_2 & q_3 \end{bmatrix}^\intercal = \begin{bmatrix} q_0 \\ \mathbf{q}_v \end{bmatrix} = \begin{bmatrix} \cos\left(\frac{\beta}{2}\right) \\ \mathbf{r}\sin\left(\frac{\beta}{2}\right) \end{bmatrix} \in \mathbf{S}^3$$

where $^\intercal$ is the transpose operator, $\mathbf{S}^3 = \{\mathbf{q} \in \mathbb{R}^4 | \mathbf{q}^\intercal\mathbf{q} = 1\}$ denotes the three-dimensional unit sphere space, q_0 and $\mathbf{q}_v = [q_1\ q_2\ q_3]^\intercal$ represent the scalar and vector parts of the unit quaternion, respectively. The norm, conjugate, and inverse of the unit quaternion $\mathbf{q}$ are defined as $\|\mathbf{q}\| = \sqrt{q_0^2 + q_1^2 + q_2^2 + q_3^2}$, $\mathbf{q}^* = [q_0\ \ -\mathbf{q}_v]^\intercal$ and $\mathbf{q}^{-1} = \frac{\mathbf{q}^*}{\|\mathbf{q}\|}$, respectively. For quaternions with $\|\mathbf{q}\| = 1$, the inverse of $\mathbf{q}$ is $\mathbf{q}^*$. The multiplication between two quaternions, $\mathbf{q}$ and $\mathbf{p} = [p_0\ \ \mathbf{p}_v]^\intercal$, which is designated by $\otimes$, is defined as [35]

$$\mathbf{q} \otimes \mathbf{p} = \begin{bmatrix} q_0 p_0 - \mathbf{q}_v^\intercal \mathbf{p}_v \\ q_0\mathbf{p}_v + p_0\mathbf{q}_v + \mathbf{q}_v \times \mathbf{p}_v \end{bmatrix}$$

where $\times$ represents the cross product. Consider a vector $\mathbf{r} \in \mathbb{R}^3$, which can be represented as $\mathbf{r}^\mathcal{I}$ in $\mathcal{I}$ and as $\mathbf{r}^\mathcal{B}$ in $\mathcal{B}$. The transformation of vector $\mathbf{r}$ from $\mathcal{B}$ to $\mathcal{I}$ is defined as

$$\begin{bmatrix} 0 \\ \mathbf{r}^\mathcal{I} \end{bmatrix} = \mathbf{q} \otimes \begin{bmatrix} 0 \\ \mathbf{r}^\mathcal{B} \end{bmatrix} \otimes \mathbf{q}^*.$$

B. Quadrotor Mathematical Model

The motion of the quadrotor is controlled by varying the speeds of four rotors. With the cooperation of four rotors, it generates one collective thrust along the negative $\boldsymbol{b}_3$ direction, which is denoted by F and three torques along the three body axes, which are τ_1, τ_2, and τ_3. The positions and velocities of the quadrotor are represented by $\boldsymbol{\xi} = [\xi_1\ \ \xi_2\ \ \xi_3]^\intercal \in \mathbb{R}^3$ and $\mathbf{v} = [v_1\ \ v_2\ \ v_3]^\intercal \in \mathbb{R}^3$, respectively. The orientation is described using a unit quaternion $\mathbf{q} = [q_0\ \ \mathbf{q}_v]^\intercal \in \mathbf{S}^3$ and the angular velocities are represented by $\boldsymbol{\omega} = [\omega_1\ \ \omega_2\ \ \omega_3]^\intercal \in \mathbb{R}^3$. Considering a quadrotor with the mass of m and the 3 by 3 inertia matrix of $\mathbf{J} \in \mathbb{R}^{3\times3}$, the dynamics can be modeled with unit quaternion formulation as [1], [25]

$$\dot{\boldsymbol{\xi}} = \mathbf{v} \tag{1}$$

$$\begin{bmatrix} 0 \\ \dot{\mathbf{v}} \end{bmatrix} = -\frac{1}{m}\mathbf{q} \otimes \begin{bmatrix} 0 \\ \mathbf{F} \end{bmatrix} \otimes \mathbf{q}^* + \begin{bmatrix} 0 \\ \mathbf{g} \end{bmatrix} + \frac{1}{m}\begin{bmatrix} 0 \\ \mathbf{d}_\xi \end{bmatrix} \tag{2}$$

$$\dot{\mathbf{q}} = \frac{1}{2}\mathbf{q} \otimes \begin{bmatrix} 0 \\ \boldsymbol{\omega} \end{bmatrix} = \frac{1}{2}\begin{bmatrix} -\mathbf{q}_v^\intercal\boldsymbol{\omega} \\ q_0\boldsymbol{\omega} + \mathbf{q}_v \times \boldsymbol{\omega} \end{bmatrix} \tag{3}$$

$$\dot{\boldsymbol{\omega}} = -\mathbf{J}^{-1}(\boldsymbol{\omega} \times \mathbf{J}\boldsymbol{\omega}) + \mathbf{J}^{-1}(\boldsymbol{\tau} + \mathbf{d}_q) \tag{4}$$

where $\mathbf{F} = [0\ \ 0\ \ F]^\intercal \in \mathbb{R}^3$ represents the thrust force vector acting on the quadrotor in $\mathcal{B}$, $\mathbf{g} = [0\ \ 0\ \ g]^\intercal \in \mathbb{R}^3$ is the gravity vector in $\mathcal{I}$, $\boldsymbol{\tau} = [\tau_1\ \ \tau_2\ \ \tau_3]^\intercal \in \mathbb{R}^3$ is the torque vector, which consists of three torques along the body axes, $\mathbf{d}_\xi \in \mathbb{R}^3$ and $\mathbf{d}_q \in \mathbb{R}^3$ are the forces and torques induced by bounded unknown external disturbances, which are acting on the position and attitude subsystems, respectively.

C. Problem Formulation

In this article, the control problem is formulated as i) developing the UDE-based global attitude control algorithms to regulate the quadrotor orientation $\mathbf{q}(t)$ to track the orientation reference $\mathbf{q}_r(t) = [q_{r0}(t)\ \ q_{r1}(t)\ \ q_{r2}(t)\ \ q_{r3}(t)]^\intercal \in \mathbf{S}^3$ for all possible initial conditions $\mathbf{q}(0)$; and ii) developing the UDE-based

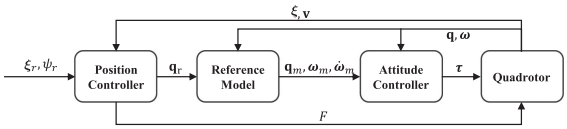

Fig. 2. Cascade control scheme for a quadrotor.

position control algorithm to drive the quadrotor position $\boldsymbol{\xi}(t)$ to track the position reference $\boldsymbol{\xi}_r(t) = [\xi_{r1}(t)\ \ \xi_{r2}(t)\ \ \xi_{r3}(t)]^\intercal \in \mathbb{R}^3$ in the presence of model uncertainties and external disturbances. The desired trajectories, $\mathbf{q}_r(t)$ and $\boldsymbol{\xi}_r(t)$ are bounded and continuously differentiable up to their second order time derivatives for all $t \geq 0$.

Remark 1: Even though the unit quaternion can represent the attitude globally without any singularity, it should be noted that there exist mechanical singularities for the quadrotor when the roll and pitch angles reach $\pm \frac{\pi}{2}$, where the total thrust has no upward component force to counter the gravity. Therefore, it is undesirable to set the unit quaternion reference $\mathbf{q}_r(t)$ to the orientation, which may result in zero upward total thrust, e.g., roll and pitch references equal to $\pm \frac{\pi}{2}$.

III. Control Design

In this section, the detailed derivations of the position control algorithms, the nonlinear reference model and the unit quaternion-based attitude controller are presented. As shown in Fig. 2, the cascade control scheme is adopted with the attitude controllers as the inner loop and the position controllers as the outer loop. Furthermore, a nonlinear reference model is employed to achieve the time-scale separation between the inner and outer loops.

A. Position Controller Design

The position and velocity tracking errors for the quadrotor are defined as

$$\begin{aligned} \boldsymbol{\xi}_e &= \boldsymbol{\xi}_r - \boldsymbol{\xi} \\ \mathbf{v}_e &= \mathbf{v}_r - \mathbf{v}. \end{aligned} \tag{5}$$

Let $\mathbf{e}_\xi = [\boldsymbol{\xi}_e\ \ \mathbf{v}_e]^\intercal$ be the error vector for the position subsystems. The objective is to design the effective position controllers to drive $\mathbf{e}_\xi$ to zero. Let $\mathbf{F}_\xi$ be the forces acting on the quadrotor in $\mathcal{I}$, where $\left[\begin{smallmatrix} 0 \\ \mathbf{F}_\xi \end{smallmatrix}\right] = \mathbf{q} \otimes \left[\begin{smallmatrix} 0 \\ \mathbf{F} \end{smallmatrix}\right] \otimes \mathbf{q}^*$. The position dynamics (2) can be rewritten in the vector form as

$$\dot{\mathbf{v}} = -\frac{1}{m}\mathbf{F}_\xi + \mathbf{g} + \frac{1}{m}\mathbf{d}_\xi. \tag{6}$$

Design the virtual control inputs as

$$\mathbf{u}_\xi = -\frac{1}{m}\mathbf{F}_\xi + \mathbf{g}. \tag{7}$$

Taking the time derivative of $\mathbf{e}_\xi$ along with (1), (5), and (6) results in

$$\dot{\mathbf{e}}_\xi = \mathbf{h}_\xi\left(\mathbf{v}_e,\ \mathbf{v}_r\right) - \mathbf{B}_\xi\left(\mathbf{u}_\xi + \frac{1}{m}\mathbf{d}_\xi\right) \tag{8}$$

where $\mathbf{h}_\xi(\mathbf{v}_e,\ \mathbf{v}_r) = [\mathbf{v}_e\ \ \dot{\mathbf{v}}_r]^\intercal \in \mathbb{R}^{6\times 3}$, $\mathbf{B}_\xi = [\mathbf{0}_{3\times 3}\ \ \mathbb{I}_3]^\intercal \in \mathbb{R}^{6\times 3}$, and $\mathbf{0}_{m\times n} \in \mathbb{R}^{m\times n}$ is m by n zero matrix. The desired error dynamics is specified as

$$\dot{\mathbf{e}}_\xi = -\mathbf{K}_\xi \mathbf{e}_\xi \tag{9}$$

where $\mathbf{K}_\xi$ is the error feedback gain matrix. Combining (8) and (9), there is

$$\mathbf{h}_\xi\left(\mathbf{v}_e,\ \mathbf{v}_r\right) - \mathbf{B}_\xi\left(\mathbf{u}_\xi + \frac{1}{m}\mathbf{d}_\xi\right) = -\mathbf{K}_\xi \mathbf{e}_\xi.$$

The control action term is designed as

$$\mathbf{B}_\xi \mathbf{u}_\xi = \mathbf{h}_\xi\left(\mathbf{v}_e,\ \mathbf{v}_r\right) + \mathbf{K}_\xi \mathbf{e}_\xi - \frac{1}{m}\mathbf{B}_\xi \mathbf{d}_\xi. \tag{10}$$

According to the position tracking error dynamics (8), the disturbance term can be solved as

$$\frac{1}{m}\mathbf{B}_\xi \mathbf{d}_\xi = \mathbf{h}_\xi\left(\mathbf{v}_e,\ \mathbf{v}_r\right) - \mathbf{B}_\xi \mathbf{u}_\xi - \dot{\mathbf{e}}_\xi.$$

The disturbance estimation is constructed following the UDE techniques in [30] by adopting strictly proper filters as

$$\frac{1}{m}\mathbf{B}_\xi \hat{\mathbf{d}}_\xi = \mathcal{L}^{-1}\left\{\mathbf{G}_{f\xi}(s)\right\} * \left[\mathbf{h}_\xi - \mathbf{B}_\xi \mathbf{u}_\xi - \dot{\mathbf{e}}_\xi\right] \tag{11}$$

where $\mathbf{G}_{f\xi}(s) \in \mathbb{R}^{6\times 6}$ is a 6 by 6 matrix in the form of $\mathbf{G}_{f\xi}(s) = \left[\begin{smallmatrix} \mathbf{0}_{3\times 3} & \mathbf{0}_{3\times 3} \\ \mathbf{0}_{3\times 3} & \mathrm{diag}(G_{f\xi 1}(s), G_{f\xi 2}(s), G_{f\xi 3}(s)) \end{smallmatrix}\right]$ and $\mathrm{diag}(\cdot)$ is the diagonal matrix operator. Replacing the disturbance term with (11) and solving for $\mathbf{u}_\xi$ leads to the UDE-based position control algorithms

$$\begin{aligned} \mathbf{u}_\xi = \mathbf{B}_\xi^+ \Big\{ & \mathcal{L}^{-1}\left\{\left(\mathbb{I}_6 - \mathbf{G}_{f\xi}(s)\right)^{-1}\right\} * \left(\mathbf{K}_\xi \mathbf{e}_\xi\right) \\ & + \mathcal{L}^{-1}\left\{\left(\mathbb{I}_6 - \mathbf{G}_{f\xi}(s)\right)^{-1}\mathbf{G}_{f\xi}(s)s\right\} * \mathbf{e}_\xi + \mathbf{h}_\xi \Big\} \end{aligned} \tag{12}$$

where $\mathbf{B}_\xi^+ = (\mathbf{B}_\xi^\intercal \mathbf{B}_\xi)^{-1}\mathbf{B}_\xi^\intercal$ denotes the pseudoinverse of $\mathbf{B}_\xi$. Then, the commanded control forces in $\mathcal{I}$ that need to be applied to the quadrotor can be solved from (7) as $\mathbf{F}_\xi = m(\mathbf{g} - \mathbf{u}_\xi)$. The magnitude of the collective thrust command is calculated as the Euclidean norm of the commanded control forces

$$F = \left\|\mathbf{F}_\xi\right\|.$$

Let the direction vector $\mathbf{r}_F$ denote the direction of commanded forces in $\mathcal{I}$, which is calculated as $\mathbf{r}_F = \frac{-\mathbf{F}_\xi}{\|\mathbf{F}_\xi\|}$. Since the thrust direction is fixed in $\mathcal{B}$, which is $-\boldsymbol{b}_3$ axis, the vector transformation from $\mathcal{B}$ to $\mathcal{I}$ can be represented as

$$\begin{bmatrix} 0 \\ \mathbf{r}_F \end{bmatrix} = \mathbf{q}_r^{b_1 b_2} \otimes \begin{bmatrix} 0 \\ -\boldsymbol{b}_3 \end{bmatrix} \otimes \left(\mathbf{q}_r^{b_1 b_2}\right)^*$$

where $\mathbf{q}_r^{b_1 b_2}$ is the desired quadrotor orientation excluding the rotation about $\boldsymbol{b}_3$ axis, which is not crucial regarding the thrust pointing direction. The unit quaternion $\mathbf{q}_r^{b_1 b_2}$ that rotates $-\boldsymbol{b}_3$ into $\mathbf{r}_F$ can be solved as [25], [36]

$$\mathbf{q}_r^{b_1 b_2} = \frac{1}{\sqrt{2\left[1 + (-\boldsymbol{b}_3)^\intercal \mathbf{r}_F\right]}} \begin{bmatrix} 1 + (-\boldsymbol{b}_3)^\intercal \mathbf{r}_F \\ (-\boldsymbol{b}_3) \times \mathbf{r}_F \end{bmatrix}. \tag{13}$$

Considering that (13) only defines the desired rotations about $\boldsymbol{b_1}$ and $\boldsymbol{b_2}$ axes, the desired orientation is fully specified as

$$\mathbf{q}_r = \mathbf{q}_r^{b_1 b_2} \otimes \left[\cos\left(\frac{\psi_r}{2}\right) \quad 0 \quad 0 \quad \sin\left(\frac{\psi_r}{2}\right)\right]^\intercal$$

where ψ_r denotes the desired heading angle.

B. Nonlinear Reference Model Design

A nonlinear reference model that observes the quaternion differential kinematics is designed in this section to smooth the control signals from the position control loop, to avoid the unreasonable attitude control inputs and to simultaneously achieve the time-scale separation between the position subsystems and attitude subsystems. Let $\mathbf{q}_m = [q_{m0} \;\; \mathbf{q}_{mv}]^\intercal$ and $\boldsymbol{\omega}_m$ denote the states of the reference model. A nonlinear reference model is designed by satisfying the unit quaternion-based attitude dynamics as [10], [30]

$$\begin{aligned}
\tilde{\mathbf{q}} &= \mathbf{q}_r^* \otimes \mathbf{q}_m = \begin{bmatrix} \tilde{q}_0 \\ \tilde{\mathbf{q}}_v \end{bmatrix} \\
\dot{\boldsymbol{\omega}}_m &= -\mathbf{A}_{m1} 2\tilde{q}_0 \tilde{\mathbf{q}}_v - \mathbf{A}_{m2}\boldsymbol{\omega}_m \\
\dot{\mathbf{q}}_m &= \frac{1}{2}\mathbf{q}_m \otimes \begin{bmatrix} 0 \\ \boldsymbol{\omega}_m \end{bmatrix}
\end{aligned} \tag{14}$$

where $\mathbf{A}_{m1}$, $\mathbf{A}_{m2}$ are 3 by 3 constant diagonal matrices and $\tilde{\mathbf{q}}$ denotes the orientation difference between $\mathbf{q}_r$ and $\mathbf{q}_m$.

C. Unit Quaternion-Based Attitude Controller Design

The attitude tracking errors $\mathbf{q}_e$ and the angular velocity tracking errors $\boldsymbol{\omega}_e$ are defined as

$$\mathbf{q}_e = \mathbf{q}_m^* \otimes \mathbf{q} = \begin{bmatrix} q_{e0} \\ \mathbf{q}_{ev} \end{bmatrix} \tag{15}$$

$$\boldsymbol{\omega}_e = \boldsymbol{\omega}_m - \boldsymbol{\omega} \tag{16}$$

where $\boldsymbol{\omega}_m = \begin{bmatrix} \omega_{m1} & \omega_{m2} & \omega_{m3} \end{bmatrix}^\intercal$, q_{e0} is the scalar part of $\mathbf{q}_e$, and $\mathbf{q}_{ev}$ is the vector part of $\mathbf{q}_e$. The unit quaternion attitude tracking error dynamics can be found via taking the time derivative of (15) [34]

$$\begin{aligned}
\dot{\mathbf{q}}_e &= -\frac{1}{2}\begin{bmatrix} 0 \\ \boldsymbol{\omega}_m \end{bmatrix} \otimes \mathbf{q}_e + \frac{1}{2}\mathbf{q}_e \otimes \begin{bmatrix} 0 \\ \boldsymbol{\omega} \end{bmatrix} \\
&= -\frac{1}{2}\begin{bmatrix} -\boldsymbol{\omega}_m^\intercal \mathbf{q}_{ev} \\ q_{e0}\boldsymbol{\omega}_m + \boldsymbol{\omega}_m \times \mathbf{q}_{ev} \end{bmatrix} + \frac{1}{2}\begin{bmatrix} -\mathbf{q}_{ev}^\intercal \boldsymbol{\omega} \\ q_{e0}\boldsymbol{\omega} + \mathbf{q}_{ev} \times \boldsymbol{\omega} \end{bmatrix} \\
&= \frac{1}{2}\begin{bmatrix} \mathbf{q}_{ev}^\intercal \boldsymbol{\omega}_m - \mathbf{q}_{ev}^\intercal \boldsymbol{\omega} \\ -q_{e0}\boldsymbol{\omega}_m + \mathbf{q}_{ev} \times \boldsymbol{\omega}_m + q_{e0}\boldsymbol{\omega} + \mathbf{q}_{ev} \times \boldsymbol{\omega} \end{bmatrix} \\
&= \frac{1}{2}\begin{bmatrix} -\mathbf{q}_{ev}^\intercal (\boldsymbol{\omega} - \boldsymbol{\omega}_m) \\ q_{e0}(\boldsymbol{\omega} - \boldsymbol{\omega}_m) + \mathbf{q}_{ev} \times (\boldsymbol{\omega} + \boldsymbol{\omega}_m) \end{bmatrix}.
\end{aligned} \tag{17}$$

Remark 2: It should be noted that in [34], the intermediate variable $\bar{\boldsymbol{\omega}}_m = R^\intercal(\mathbf{q}_e)\boldsymbol{\omega}_m$, where $R(\mathbf{q}_e)$ is the rotation matrix calculated from the unit quaternion $\mathbf{q}_e$, is introduced to facilitate the controller derivation. While in this article, (17) is derived without introducing any intermediate variable. As a result, it avoids the computation of the rotation matrix while preserving the advantage of the quaternion in terms of computational efficiency.

From (4), (16), and (17), the tracking error dynamics for attitude subsystems can be written in the form of

$$\begin{aligned}
\dot{\mathbf{q}}_e &= \frac{1}{2}\begin{bmatrix} -\mathbf{q}_{ev}^\intercal (\boldsymbol{\omega} - \boldsymbol{\omega}_m) \\ q_{e0}(\boldsymbol{\omega} - \boldsymbol{\omega}_m) + \mathbf{q}_{ev} \times (\boldsymbol{\omega} + \boldsymbol{\omega}_m) \end{bmatrix} \\
\dot{\boldsymbol{\omega}}_e &= \dot{\boldsymbol{\omega}}_m + \mathbf{J}^{-1}(\boldsymbol{\omega} \times \mathbf{J}\boldsymbol{\omega}) - \mathbf{J}^{-1}(\boldsymbol{\tau} + \mathbf{d}_q).
\end{aligned} \tag{18}$$

The objective is to design the effective attitude controllers, which are capable of driving the quaternion attitude tracking errors $\mathbf{q}_e$ to $[\pm 1 \;\; 0 \;\; 0 \;\; 0]^\top$ and the angular velocity tracking errors $\boldsymbol{\omega}_e$ to zero. It should be noted that $\mathbf{q}_e = [1 \;\; 0 \;\; 0 \;\; 0]^\intercal$ and $\mathbf{q}_e = [-1 \;\; 0 \;\; 0 \;\; 0]^\intercal$ correspond to the scenarios where the differences between $\mathbf{q}_m$ and $\mathbf{q}$ are 0° and 360°, respectively, which are the same physical attitude [20], [24]. Therefore, the two equilibrium points $\mathbf{q}_e = [\pm 1 \;\; 0 \;\; 0 \;\; 0]^\top$ are in reality one physical equilibrium point.

Remark 3: It can be observed that the quaternion-based attitude error dynamics (18) is highly nonlinear with the equilibrium points of $[\pm 1 \;\; 0 \;\; 0 \;\; 0]^\top$. Therefore, it may be difficult to directly derive the UDE-based controller from (18). Inspired by [33], the backstepping technique is adopted to deal with the highly nonlinear quaternion-based error dynamics along with the following coordinate transformation:

$$\begin{aligned}
\mathbf{z}_1 &= \mathbf{q}_{ev} \\
\mathbf{z}_2 &= -\boldsymbol{\omega}_e + \boldsymbol{\alpha}
\end{aligned} \tag{19}$$

where $\boldsymbol{\alpha}$ is the virtual control to be designed. Due to the unity property of $\mathbf{q}_e$, if $\mathbf{z}_1 = \mathbf{q}_{ev}$ converges to zero, then q_{e0} will converge to ± 1.

Design the virtual control as [10]

$$\boldsymbol{\alpha} = 2\mathbf{C}_1 q_{e0}\mathbf{q}_{ev} \tag{20}$$

where $\mathbf{C}_1 \in \mathbb{R}^{3\times 3}$ is a 3 by 3 positive constant matrix. It should be noted that the unwinding problem, where the quaterinon double covers the physical attitude space, is tackled with the introduction of the virtual controller (20). Taking the time derivative of (19) leads to

$$\begin{aligned}
\dot{\mathbf{z}}_1 &= -\frac{1}{2}q_{e0}\boldsymbol{\omega}_e + \frac{1}{2}\mathbf{z}_1 \times (\boldsymbol{\omega} + \boldsymbol{\omega}_m) + \frac{1}{2}q_{e0}\boldsymbol{\alpha} - \frac{1}{2}q_{e0}\boldsymbol{\alpha} \\
&= -q_{e0}^2\mathbf{C}_1\mathbf{z}_1 + \frac{1}{2}q_{e0}\mathbf{z}_2 + \frac{1}{2}\mathbf{z}_1 \times (\boldsymbol{\omega} + \boldsymbol{\omega}_m)
\end{aligned} \tag{21}$$

$$\begin{aligned}
\dot{\mathbf{z}}_2 &= -\dot{\boldsymbol{\omega}}_e + \dot{\boldsymbol{\alpha}} \\
&= -\dot{\boldsymbol{\omega}}_m - \mathbf{J}^{-1}(\boldsymbol{\omega} \times \mathbf{J}\boldsymbol{\omega}) + \mathbf{J}^{-1}(\boldsymbol{\tau} + \mathbf{d}_q) + \dot{\boldsymbol{\alpha}}.
\end{aligned} \tag{22}$$

Choosing the Lyapunov function candidate as

$$V_q = \frac{1}{2}\mathbf{z}_1^\intercal \mathbf{z}_1 + \frac{1}{2}\mathbf{z}_2^\intercal \mathbf{z}_2. \tag{23}$$

Taking the time derivative of (23) results in

$$\begin{aligned}\dot{V}_q &= \mathbf{z}_1^\intercal \dot{\mathbf{z}}_1 + \mathbf{z}_2^\intercal \dot{\mathbf{z}}_2 \\ &= \mathbf{z}_1^\intercal \left[-q_{e0}^2 \mathbf{C}_1 \mathbf{z}_1 + \frac{1}{2} q_{e0} \mathbf{z}_2 + \frac{1}{2} \mathbf{z}_1 \times (\boldsymbol{\omega} + \boldsymbol{\omega}_m) \right] + \mathbf{z}_2^\intercal \dot{\mathbf{z}}_2 \end{aligned} \tag{24}$$

$$= -\mathbf{z}_1^\intercal q_{e0}^2 \mathbf{C}_1 \mathbf{z}_1 + \mathbf{z}_2^\intercal \left(\frac{1}{2} q_{e0} \mathbf{z}_1 + \dot{\mathbf{z}}_2 \right). \tag{25}$$

In order to facilitate derivation, the cross product term in (24) can be rewritten in matrix multiplication form as

$$\frac{1}{2} \mathbf{z}_1^\intercal \mathbf{z}_1 \times (\boldsymbol{\omega} + \boldsymbol{\omega}_m) = \frac{1}{2} \mathbf{z}_1^\intercal \left[\mathbf{S}(\mathbf{z}_1) (\boldsymbol{\omega} + \boldsymbol{\omega}_m) \right] \tag{26}$$

where $\mathbf{S}(\mathbf{z}_1)$ represents the skew-symmetric matrix in the form of

$$\mathbf{S}(\mathbf{z}_1) = \begin{bmatrix} 0 & -z_{13} & z_{12} \\ z_{13} & 0 & -z_{11} \\ -z_{12} & z_{11} & 0 \end{bmatrix}$$

and $\mathbf{z}_1 = \begin{bmatrix} z_{11} & z_{12} & z_{13} \end{bmatrix}^\intercal$. Expanding (26) leads to zero. To ensure (25) is negative, the desired error dynamics is

$$\frac{1}{2} q_{e0} \mathbf{z}_1 + \dot{\mathbf{z}}_2 = -\mathbf{C}_2 \mathbf{z}_2 \tag{27}$$

where $\mathbf{C}_2 \in \mathbb{R}^{3\times 3}$ is a 3 by 3 positive gain matrix. Combining (22) and (27), the control action term is designed as

$$\mathbf{J}^{-1} \boldsymbol{\tau} = -\mathbf{C}_2 \mathbf{z}_2 - \frac{1}{2} q_{e0} \mathbf{z}_1 + \dot{\boldsymbol{\omega}}_m + \mathbf{J}^{-1} (\boldsymbol{\omega} \times \mathbf{J}\boldsymbol{\omega}) - \mathbf{u}_d \tag{28}$$

where $\mathbf{u}_d = \mathbf{J}^{-1}\mathbf{d}_q + \dot{\boldsymbol{\alpha}}$ is the lumped uncertainty term. The lumped uncertainty term can be solved from (22) as

$$\mathbf{u}_d = \dot{\mathbf{z}}_2 + \dot{\boldsymbol{\omega}}_m + \mathbf{J}^{-1} (\boldsymbol{\omega} \times \mathbf{J}\boldsymbol{\omega}) - \mathbf{J}^{-1}\boldsymbol{\tau}. \tag{29}$$

Following the UDE techniques provided in [30], by adopting strictly proper filters with unity steady-state gains, the lumped uncertainty term can be estimated as

$$\begin{aligned}\hat{\mathbf{u}}_d = \mathcal{L}^{-1} \{ \mathbf{G}_{fq}(s) \} * \{ &\dot{\mathbf{z}}_2 + \dot{\boldsymbol{\omega}}_m \\ &+ \mathbf{J}^{-1} (\boldsymbol{\omega} \times \mathbf{J}\boldsymbol{\omega}) - \mathbf{J}^{-1}\boldsymbol{\tau} \}\end{aligned} \tag{30}$$

where $\mathcal{L}^{-1}$ is the inverse Laplace operator, $*$ is the convolution operator, $\hat{\mathbf{u}}_d$ represents the estimation of lumped uncertainty term $\mathbf{u}_d$, and $\mathbf{G}_{fq}(s) \in \mathbb{R}^{3\times 3}$ is a 3 by 3 filter matrix in the form of $\mathbf{G}_{fq}(s) = \text{diag}(G_{fq1}(s),\ G_{fq2}(s),\ G_{fq3}(s))$. Substituting (30) back into (28) and solving for $\boldsymbol{\tau}$, the UDE-based attitude control laws are derived as

$$\begin{aligned}\boldsymbol{\tau} = &\boldsymbol{\omega} \times \mathbf{J}\boldsymbol{\omega} + \mathbf{J}\dot{\boldsymbol{\omega}}_m \\ &- \mathbf{J}\mathcal{L}^{-1} \left\{ \left(\mathbb{I}_3 - \mathbf{G}_{fq}(s) \right)^{-1} \right\} * \left[\mathbf{C}_2 \mathbf{z}_2 + \frac{1}{2} q_{e0} \mathbf{z}_1 \right] \\ &- \mathbf{J}\mathcal{L}^{-1} \left\{ \left(\mathbb{I}_3 - \mathbf{G}_{fq}(s) \right)^{-1} \mathbf{G}_{fq}(s) s \right\} * \mathbf{z}_2 \end{aligned} \tag{31}$$

where $\mathbb{I}_n \in \mathbb{R}^{n\times n}$ is the n-dimensional identity matrix.

Assumption 1: For the controller implementation, it is assumed that the nominal value of the inertia matrix $\mathbf{J}$ is known.

It should be noted that the Assumption 1 can be easily satisfied with the system identification technique in [37].

IV. Stability Analysis

In this section, the stability of closed-loop attitude subsystems with the developed unit quaternion-based attitude controllers are analyzed. The stability analysis of the position subsystems can be conducted following the similar procedures provided in [19].

Substituting (28), (30), into (22) results in the closed-loop error dynamics for attitude subsystems

$$\begin{aligned}\dot{\mathbf{z}}_1 &= -q_{e0}^2 \mathbf{C}_1 \mathbf{z}_1 + \frac{1}{2} q_{e0} \mathbf{z}_2 + \frac{1}{2} \mathbf{z}_1 \times (\boldsymbol{\omega} + \boldsymbol{\omega}_m) \\ \dot{\mathbf{z}}_2 &= -\mathbf{C}_2 \mathbf{z}_2 - \frac{1}{2} q_{e0} \mathbf{z}_1 + \tilde{\mathbf{u}}_d \end{aligned} \tag{32}$$

where $\tilde{\mathbf{u}}_d = \mathcal{L}^{-1}(\mathbb{I}_3 - \mathbf{G}_{fq}(s)) * \mathbf{u}_d$ is the lumped uncertainty estimation error vector for attitude subsystems. Combining (32) and (25) leads to

$$\begin{aligned}\dot{V}_q &= \mathbf{z}_1^\intercal \dot{\mathbf{z}}_1 + \mathbf{z}_2^\intercal \dot{\mathbf{z}}_2 \\ &= -q_{e0}^2 \mathbf{z}_1^\intercal \mathbf{C}_1 \mathbf{z}_1 - \mathbf{z}_2^\intercal \mathbf{C}_2 \mathbf{z}_2 + \mathbf{z}_2^\intercal \tilde{\mathbf{u}}_d \\ &\leq -q_{e0}^2 \mathbf{z}_1^\intercal \mathbf{C}_1 \mathbf{z}_1 - \lambda_{\min}(\mathbf{C}_2)(1-\Theta) \|\mathbf{z}_2\|^2 \\ &\quad - \lambda_{\min}(\mathbf{C}_2) \Theta \|\mathbf{z}_2\|^2 + \|\mathbf{z}_2\| \|\tilde{\mathbf{u}}_d\| \end{aligned} \tag{33}$$

where $0 < \Theta < 1$ is a constant, $\lambda_{\min}(\cdot)$ denotes the minimum eigenvalue of a matrix. Then,

$$\begin{aligned}\dot{V}_q \leq &-q_{e0}^2 \mathbf{z}_1^\intercal \mathbf{C}_1 \mathbf{z}_1 - \lambda_{\min}(\mathbf{C}_2)(1-\Theta) \|\mathbf{z}_2\|^2 \leq 0 \\ &\forall \|\mathbf{z}_2\| \geq \frac{\|\tilde{\mathbf{u}}_d\|}{\lambda_{\min}(\mathbf{C}_2)\Theta}. \end{aligned} \tag{34}$$

Therefore, if the filter matrix $\mathbf{G}_{fq}(s)$, controller parameter matrix $\mathbf{C}_2$ and constant Θ are chosen properly to satisfy the derived condition $\|\mathbf{z}_2\| \geq \frac{\|\tilde{\mathbf{u}}_d\|}{\lambda_{\min}(\mathbf{C}_2)\Theta}$, there exists an invariant set $\Omega_q = \{V_q \in \mathbb{R} : V_q \leq \delta\}$ such that V_q with initial conditions $V_q(0)$ in Ω_q will remain in Ω_q for all $t \geq 0$ with δ being the upper bound of V_q. Then, the closed-loop system tracking errors $\mathbf{z}_1$ and $\mathbf{z}_2$ are uniformly bounded. Furthermore, from the invertible change of coordinates (19), it can be concluded that $\mathbf{q}_{ev}$ and $\boldsymbol{\omega}_e$ are uniformly bounded.

The derivative of the virtual control can be calculated from (20) as $\dot{\boldsymbol{\alpha}} = 2\mathbf{C}_1 \dot{q}_{e0} \mathbf{q}_{ev} + 2\mathbf{C}_1 q_{e0} \dot{\mathbf{q}}_{ev}$. From (17), it can be observed that $\dot{q}_{e0}$ and $\dot{\mathbf{q}}_{ev}$ are continuous functions of $\mathbf{q}_{ev}$, q_{e0}, $\boldsymbol{\omega}$, $\boldsymbol{\omega}_m$. Since $\mathbf{q}_{ev}$ and q_{e0} are structurally bounded and $\boldsymbol{\omega}$ is bounded from the boundness of $\boldsymbol{\omega}_e$ and $\boldsymbol{\omega}_m$, then $\dot{\boldsymbol{\alpha}}$ is bounded. From the definition of the lumped uncertainty term, $\mathbf{u}_d = \mathbf{J}^{-1}\mathbf{d}_q + \dot{\boldsymbol{\alpha}}$, where $\mathbf{d}_q$ is the bounded external disturbance. Then, it can be concluded that $\mathbf{u}_d$ is bounded. By adopting the diagonal filter matrix $\mathbf{G}_{fq}(s) = \text{diag}(G_{fq1}(s),\ G_{fq2}(s),\ G_{fq3}(s))$, which has the diagonal elements as strictly proper stable filters with all the poles on the left-hand side of the complex plane, the estimation error vector $\tilde{\mathbf{u}}_d = \mathcal{L}^{-1}(\mathbb{I}_3 - \mathbf{G}_{fq}(s)) * \mathbf{u}_d$ is also bounded with $\|\tilde{\mathbf{u}}_d\| \leq \gamma$, where γ is a constant.

To determine the bound of the invariant set Ω_q, applying Young's inequality to (33) along with (23), there is

$$\begin{aligned}\dot{V}_q &\le -q_{e0}^2\lambda_{\min}(\mathbf{C}_1)\|\mathbf{z}_1\|^2 - \lambda_{\min}(\mathbf{C}_2)\|\mathbf{z}_2\|^2 \\ &\quad + \frac{1}{2}\|\mathbf{z}_2\|^2 + \frac{1}{2}\|\tilde{\mathbf{u}}_d\|^2 \\ &\le -2\mu V_q + \frac{1}{2}\gamma^2 \end{aligned} \tag{35}$$

where $\mu = \min\{q_{e0}^2\lambda_{\min}(\mathbf{C}_1),\ [\lambda_{\min}(\mathbf{C}_2) - \frac{1}{2}]\} > 0$ in the case of $q_{e0} \neq 0$. The special case when $q_{e0} = 0$ will be discussed latter. Solving (35) results in

$$V_q \le V_q(0)e^{-2\mu t} + \frac{\gamma^2}{4\mu}\left(1 - e^{-2\mu t}\right). \tag{36}$$

Therefore, the upper bound of V_q can be calculated as $\delta = \max\{V_q(0),\ \frac{\gamma^2}{4\mu}\}$. The bound is determined by the initial condition $V_q(0)$, the controller parameters $\mathbf{C}_1$, $\mathbf{C}_2$ and the estimation error vector $\tilde{\mathbf{u}}_d$. As $t \to \infty$, the first term on the right-hand side of (36) will decay to 0, and the second term is bounded by $\frac{\gamma^2}{4\mu}$. The size of the bound can be adjusted as small as possible by tuning the controller parameters $\mathbf{C}_1$, $\mathbf{C}_2$ and properly designing the filter matrix $\mathbf{G}_{fq}(s)$. The guideline for the filter design to achieve the asymptotic disturbance rejection performance is discussed in [31].

It should be noted that there is a special case when $q_{e0} = 0$, where $\mathbf{q}_m$ and $\mathbf{q}$ are 180° away. When $q_{e0} = 0$ and $\boldsymbol{\omega}_e$ are a zero vector, $\mathbf{q}_e$ will be a constant unit quaternion, which is structurally bounded. Therefore, it can be concluded that closed-loop system tracking errors $\mathbf{z}_1$ and $\boldsymbol{\omega}_e$ are bounded. If $\boldsymbol{\omega}_e$ is a nonzero vector, the nonzero $\boldsymbol{\omega}_e$ will drive $\mathbf{q}_e$ to leave the point of $q_{e0} = 0$, then the above mentioned conclusions derived in the case of $q_{e0} \neq 0$ can be applied.

V. Experiments

In this section, the flight experiments are carried out to validate the effectiveness of the developed unit quaternion-based robust control strategies. Three experimental cases are considered, which are attitude recovery, trajectory tracking with wind disturbance, and comparison with the existing robust controller [1], to demonstrate the capability of developed controller for large angle maneuvers and accurate trajectory tracking under the influence of external disturbance and the superior robustness of the proposed approach over existing controller in handling model uncertainty and disturbance.

A. Experimental Setup

The quadrotor platform used in experiments is a Parrot Mambo quadrotor, which is shown in Fig. 3. The weight of the quadrotor is about 63 g. The orientation estimation is carried out with measurements provided by a three-axis accelerometer and a three-axis gyroscope. An ultrasonic sensor, an air pressure sensor, and a downward-facing camera are used for relative position localization. The control loop is running with the update rate of 200 Hz. The flight control algorithm programming is done with Simulink Support Package [38]. The experimental environment is shown in Fig. 4.

(a) (b)

Fig. 3. Experimental platform. (a) Top view. (b) Bottom view.

Fig. 4. Experimental environment.

B. Controller Parameter Selection

For implementation, the low-pass filter matrices in (12) and (31) are chosen as [30], [31]

$$\mathbf{G}_{f\xi}(s) = \begin{bmatrix} \mathbf{0}_{3\times3} & \mathbf{0}_{3\times3} \\ \mathbf{0}_{3\times3} & \operatorname{diag}\left(\frac{1}{T_{\xi1}s+1}, \frac{1}{T_{\xi2}s+1}, \frac{1}{T_{\xi3}s+1}\right) \end{bmatrix}$$

$$\mathbf{G}_{fq}(s) = \operatorname{diag}\left(\frac{1}{T_{q1}s+1}, \frac{1}{T_{q2}s+1}, \frac{1}{T_{q3}s+1}\right).$$

The matrix $\mathbf{K}_\xi$ in (12) are designed as $\begin{bmatrix} \mathbf{0}_{3\times3} & \mathbb{I}_3 \\ \mathbf{K}_1 & \mathbf{K}_2 \end{bmatrix}$ with $\mathbf{K}_1$ and $\mathbf{K}_2$ being the 3 by 3 diagonal matrices in the form of

$$\mathbf{K}_1 = \operatorname{diag}(k_{11},\ k_{12},\ k_{13}),\ \mathbf{K}_2 = \operatorname{diag}(k_{21},\ k_{22},\ k_{23}).$$

The constant matrices $\mathbf{A}_{m1}$ and $\mathbf{A}_{m2}$ for the developed nonlinear reference model are also chosen as diagonal matrices in the forms of

$$\mathbf{A}_{m1} = \operatorname{diag}(a_{m11},\ a_{m12},\ a_{m13})$$
$$\mathbf{A}_{m2} = \operatorname{diag}(a_{m21},\ a_{m22},\ a_{m23}).$$

The matrices $\mathbf{C}_1$ and $\mathbf{C}_2$ in (31) are chosen as diagonal matrices in the forms of

$$\mathbf{C}_1 = \operatorname{diag}(c_{11},\ c_{12},\ c_{13}),\ \mathbf{C}_2 = \operatorname{diag}(c_{21},\ c_{22},\ c_{23}).$$

The selections of parameters are listed in Table I.

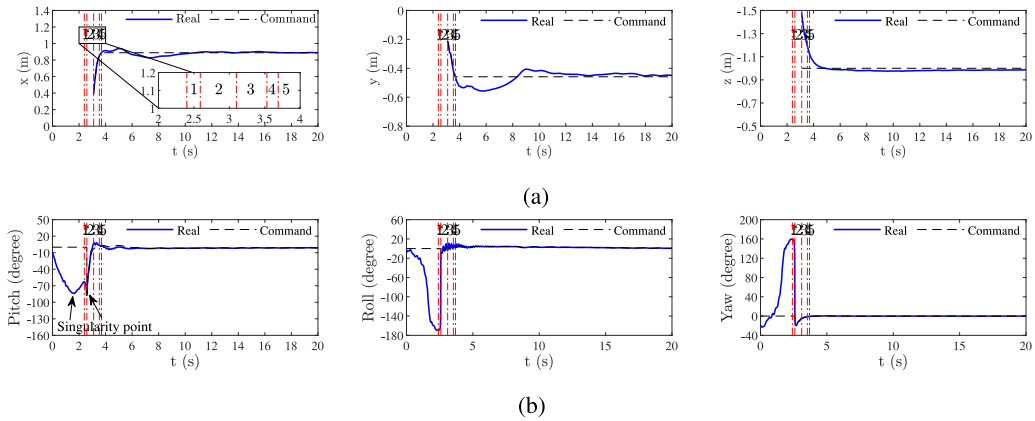

Fig. 5. Case I: Attitude recovery with five stages: 1: launch detection, 2: attitude control enabled, 3: height control enabled, 4: horizontal velocity control enabled, 5: full DOF control enabled. (a) Positions. (b) Euler angles.

TABLE I
CONTROLLER PARAMETER SELECTION

	T_{qi}	c_{1i}	c_{2i}	$T_{\xi i}$	k_{1i}	k_{2i}	a_{m1i}	a_{m2i}
1	1/60	1	2	1/40	1	2	100	20
2	1/50	1	2	1/40	1	2	100	20
3	1/20	1	2	1/20	1	2	25	10

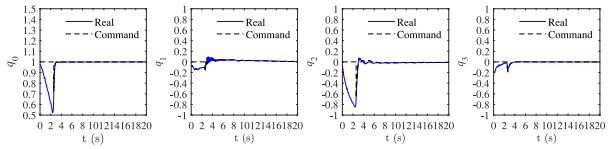

Fig. 6. Case I: Attitude recovery: quaternion.

C. Results and Discussion

1) Case I. Attitude Recovery: In this case, the control objective is to achieve attitude recovery and position hover under random initial conditions, which are generated by hand tossing. This experimental case is performed by throwing the quadrotor by hand in an indoor environment, where the sensing is conducted with onboard sensors and no disturbance is applied. After the quadrotor is thrown, the launch detection, attitude recovery, and position holding are achieved autonomously. The similar launch detection and recovery processes in [39] are adopted, which consist of five stages.

The first stage is the launch detection, which is achieved by analyzing the accelerometer data. Let $\|a\|$ denote the averaged norm of accelerometer data within last 20 ms. After the quadrotor is released by hand, it will start falling freely, where $\|a\|$ will approach zero. When $\|a\|$ is less than the threshold of 3 $\mathrm{m/s^2}$, the attitude recovery process will be initiated, which is the second stage. In the second stage, the attitude controllers and the nonlinear reference model are enabled to control the quadrotor attitude to the level with the attitude references set as $\mathbf{q}_r = [1\ \ 0\ \ 0\ \ 0]^\intercal$. The initial conditions of the nonlinear reference model are set as the current orientations of the quadrotor when the second stage is initiated. Based on the quadrotor nominal weight, the quadrotor thrust is set as $F = mg$. When the quadrotor roll and pitch angles are less than 10° and the roll and pitch angular velocities are less than 1 rad/s, the third stage will be switched ON. The height controller is enabled in the third stage with the reference set as -1 m. Since $\boldsymbol{i}_3$ is pointing downward, the negative value actually means the quadrotor is above the ground. Once the height controller is enabled and the vertical velocity is less than 0.5 m/s, the fourth stage is enabled to reduce the horizontal velocities. In the fourth stage, the horizontal position controllers are activated with only velocity measurements feeding to the controllers while the velocity references are set as zero. As soon as the horizontal velocities are small enough, i.e., $\|v_1\| \leq 0.2$ m/s and $\|v_2\| \leq 0.2$ m/s, the full DOF control of quadrotor is initiated with the horizontal position references set as current positions.

The experimental results are shown in Fig. 5 with different stages marked. The positions are plotted as x, y, z, and the orientations are shown as Euler angles for reader-friendly presentation. Since the quadrotor measures positions with respect to ground, the measurements before stage 2 are not plotted, which are not able to accurately reflect the quadrotor positions. The quadrotor attitude in terms of unit quaternion is shown in Fig. 6. The quadrotor is hand tossed at around $t = 2.4$ s, where the attitude are -159.556° in roll direction, -62.748° in pitch direction, -169.603° in yaw direction in terms of Euler angle representation.

Remark 4: It should be noted when the quadrotor is tossed, the pitch angle has already passed the mathematical and mechanical singularity point, which is -90° at $t = 1.62$ s, as shown in Fig. 5(b). In terms of rotation about the $\boldsymbol{b_2}$ axis, the angle is actually -117.252° at $t = 2.4$ s. It can also be observed from q_2 in Fig. 6 that the quadrotor is rotating by hand in one direction before tossed. However, the mathematical singularity in Euler angle representation limits the pitch angle within the range of $\pm 90^\circ$ and results in sudden jumps in roll and yaw angles when pitch angle passes through $\pm 90^\circ$.

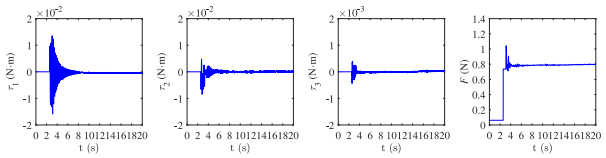

Fig. 7. Case I: Attitude recovery: control inputs.

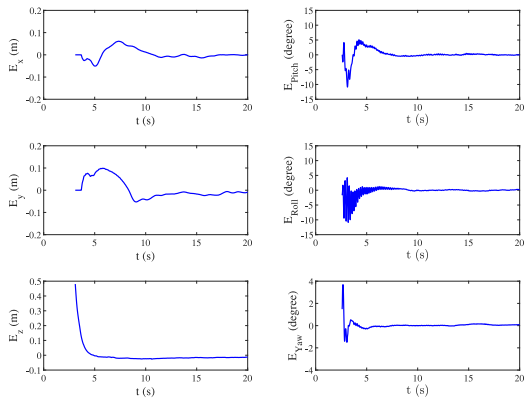

(a) (b)

Fig. 8. Case I: Attitude recovery. (a) Position tracking errors. (b) Euler angle tracking errors.

TABLE II
RMSEs OF THE EXPERIMENTAL RESULTS

	Case I (15:35 s)	Case II
x (m)	0.005	0.058
y (m)	0.013	0.038
z (m)	0.013	0.020
roll (degree)	0.257	0.945
pitch (degree)	0.148	1.365
yaw (degree)	0.093	0.588

The evolution of control inputs are shown in Fig. 7. The period of experimental case I is about 35 s. Only the results from 0 to 20 s are plotted for a better view of the recovery processes. Define the position tracking errors as $\mathrm{E_x}$, $\mathrm{E_y}$, $\mathrm{E_z}$ and the attitude tracking errors as $\mathrm{E_{Roll}}$,$\mathrm{E_{Pitch}}$, $\mathrm{E_{Yaw}}$. The position and Euler angle tracking errors are shown in Fig. 8. To have a better view of the performance of the proposed control strategy, the position tracking errors are shown started from stage 3, when the height controller is enabled and the attitude tracking errors are shown started from stage 2, when the attitude controllers are enabled. The steady-state root-mean-square errors (RMSEs) from 15 to 35 s when the quadrotor is stably hovering are calculated in Table II. The experimental results have demonstrated the singularity-free property of the proposed approach by accomplishing large angle maneuvers and the stability of the proposed approach under undesirable initial conditions.

2) Case II. Trajectory Tracking With Wind Disturbance: The control objective of the second case is to let the quadrotor track the desired trajectory in presence of external wind disturbances. The reference trajectory is designed as a Lissajous curve in the form of $\boldsymbol{\xi}_r = [\sin(0.5t)\ \ \sin(0.25t)\ \ -1]^\intercal$ m. The wind disturbances are generated by a fan, which is shown in Fig. 4. An AR816 digital anemometer from Smart Sensor[1] is used to measure the generated wind profile. The wind speed measurement is carried out by placing the anemometer at the point of $[0\ \ 0\ \ -1]^\intercal$ m. The measured average wind speed over two minutes is 1.6 m/s. The experimental results are shown in Figs. 9–11. The tracking errors for all DOFs are plotted in Fig. 12. The calculated RMSEs are listed in Table II, which are quite small considering the small mass of the experimental platform (less than 100 g) and the time-varying and location-dependent properties of the generated wind field. The experimental results successfully validate that the quadrotor can accurately track the desired trajectory even in the presence of external disturbances while demonstrating the robustness of the developed control strategies.

3) Case III. Comparison With the Existing Robust Controller [1]: To demonstrate the advantages of the proposed controller, the comparative experiments with the quaternion-based robust strategy, which is developed in [1] are carried out. The control objective of the third case is to let the quadrotor track the desired trajectory in presence of model uncertainties and disturbances. The reference trajectory is the same with the Case II. Let $\odot$ and $\oslash$ denote the component multiplication and division for vectors. For example, define the two vectors, respectively, as $\mathbf{r} = [r_1\ \ r_2\ \ r_3]^\intercal \in \mathbb{R}^3$ and $\mathbf{s} = [s_1\ \ s_2\ \ s_3]^\intercal \in \mathbb{R}^3$, then the component multiplication is calculated as $\mathbf{r} \odot \mathbf{s} = [r_1 s_1\ \ r_2 s_2\ \ r_3 s_3]^\intercal \in \mathbb{R}^3$. In [1], the hybrid robust controllers for the quadrotor are developed in the form of

$$\begin{aligned}\mathbf{F}_\xi &= m\mathbf{g} - m\ddot{\boldsymbol{\xi}}_r + \boldsymbol{\lambda}_2 \odot \sigma\left(\boldsymbol{k}_2 \oslash \boldsymbol{\lambda}_2 \odot \left(\mathbf{v}_e\right.\right.\\ &\quad \left.\left. + \ \boldsymbol{\lambda}_1 \odot \sigma\left(\boldsymbol{k}_1 \oslash \boldsymbol{\lambda}_1 \odot \boldsymbol{\xi}_e\right)\right)\right)\\ \boldsymbol{\tau} &= \mathbf{J}\dot{\boldsymbol{\omega}}_r - \mathbf{S}\left(\mathbf{J}\boldsymbol{\omega}_r\right)\boldsymbol{\omega}_r - h\boldsymbol{k}_p \odot \mathbf{q}_{ev} - \boldsymbol{k}_p \odot \boldsymbol{k}_d \odot \tilde{\boldsymbol{\omega}}^*\end{aligned}$$

where $\mathbf{F}_\xi$ is the vector of the position controllers, $\boldsymbol{\tau}$ is the vector of the attitude controllers, $\boldsymbol{\omega}_r$ is the reference angular velocity, $\tilde{\boldsymbol{\omega}}^* = \boldsymbol{\omega} - \bar{\boldsymbol{\omega}}_r$, $\bar{\boldsymbol{\omega}}_r = R(\mathbf{q}_e)\boldsymbol{\omega}_r$, $R(\mathbf{q}_e)$ is the rotation matrix calculated from the unit quaternion $\mathbf{q}_e$, $h \in \{-1,\ 1\}$ which is governed by the following hybrid dynamics

$$\begin{cases}\dot{h} = 0 & hq_{e0} \geq -\delta \text{ or } \mathbf{q}_{ev}\mathbf{J}^U\mathbf{q}_{ev}\\ & \quad + \tilde{\boldsymbol{\omega}}^*\mathbf{J}^U\tilde{\boldsymbol{\omega}}^* \geq 2\boldsymbol{k}_d\delta\\ h^+ \in \bar{\mathrm{sgn}}\left(q_{e0}\right) & hq_{e0} \leq -\delta,\ \mathbf{q}_{ev}\mathbf{J}^U\mathbf{q}_{ev}\\ & \quad + \tilde{\boldsymbol{\omega}}^*\mathbf{J}^U\tilde{\boldsymbol{\omega}}^* \leq 2\boldsymbol{k}_d\delta\end{cases}$$

$\bar{\mathrm{sgn}}(\cdot)$ and $\sigma(\cdot)$ are, respectively, the sign and saturation functions defined in [1]. The controller parameters are set as $\boldsymbol{k}_1 = [70\ \ 70\ \ 10]^\intercal$, $\boldsymbol{k}_2 = [0.01\ \ 0.01\ \ 0.3]^\intercal$, $\boldsymbol{\lambda}_1 = [10\ \ 10\ \ 10]^\intercal$, $\boldsymbol{\lambda}_2 = [10\ \ 10\ \ 10]^\intercal$, $\delta = 0.15$, $\mathbf{J}^U = \mathrm{diag}(0.01,\ 0.01,\ 0.02)$, $\boldsymbol{k}_p = [0.03\ \ 0.03\ \ 0.01]^\intercal$, $\boldsymbol{k}_d = [0.06\ \ 0.06\ \ 0.02]^\intercal$. It should be noted that compared to the controller developed in [1], the proposed control algorithms avoid the calculation of the rotation matrix. Therefore, the proposed controllers are computationally

[1][Online]. Available: http://en.smartsensor.cn/

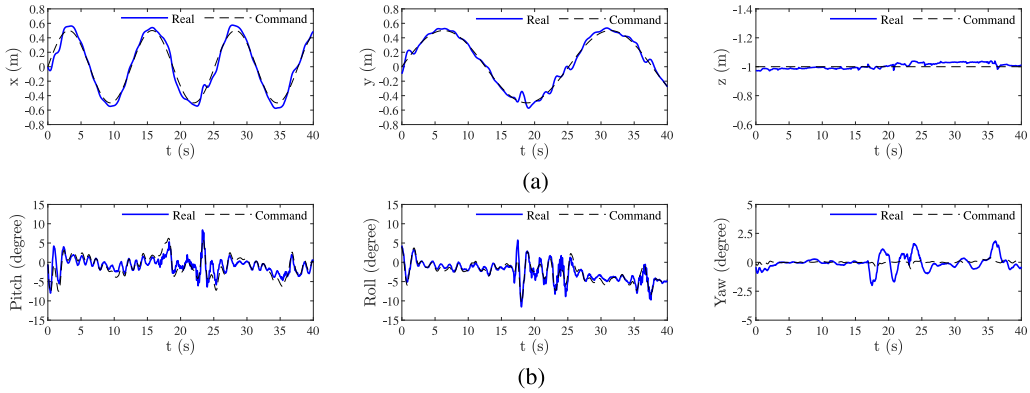

Fig. 9. Case II: Trajectory tracking with wind disturbance. (a) Positions. (b) Euler angles.

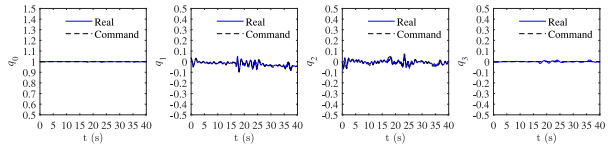

Fig. 10. Trajectory tracking with wind disturbance: quaternion.

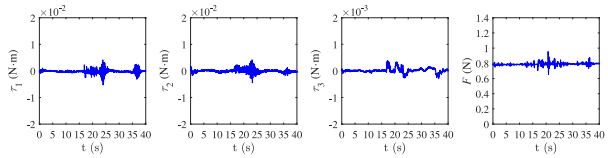

Fig. 11. Case II: Trajectory tracking with wind disturbance: control inputs.

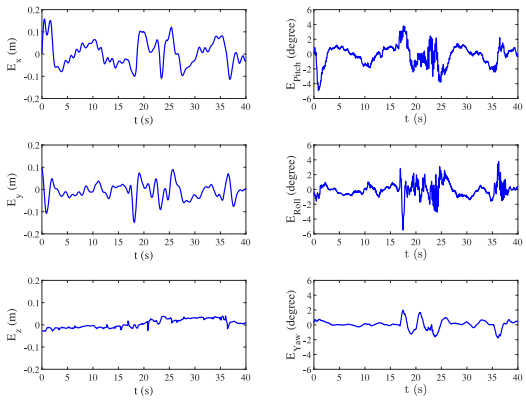

Fig. 12. Case II: Trajectory tracking with wind disturbance. (a) Position tracking errors. (b) Euler angle tracking errors.

more efficient. To ensure the fair comparison, the nominal scenario is carried out without any uncertainty and disturbance. The control parameters of the robust controller developed in [1] are tuned to achieve the best possible performance. As shown in Fig. 14(a), the performances of the proposed controller, which are plotted with blue thick solid line and the performances of

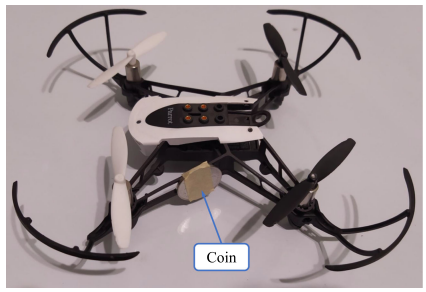

Fig. 13. Model uncertainty with additional coin attached.

the robust controller developed in [1], which are plotted with red thin solid line are similar in the nominal scenario. Then, the uncertainty and disturbance rejection scenario is considered with the controller parameters unchanged. As shown in Fig. 13, a coin with the weight of 6 g, which are about 10% of the quadrotor's weight, is added to the side of the quadrotor as model uncertainties before take-off. The added coin is unknown to the controllers and it changes the quadrotor's weight and inertia. In particular, the asymmetry weight distribution largely changes the quadrotor's inertia along the $\boldsymbol{b_1}$ axis. The input step disturbances with the magnitude of $0.002\ \mathrm{N}\cdot\mathrm{m}$ are added to the roll and pitch directions at $t = 20$ s. The position and attitude tracking performances for the uncertainty and disturbance rejection scenario are shown in Fig. 14(b). For the controller developed in [1], it can be clearly seen that due to added model uncertainties, the quadrotor slightly deviates from the references for the roll and y directions. After the disturbance is added at $t = 20$ s, though the controller developed in [1] can still track the references, the tracking performances are deteriorated in roll, pitch, x and y directions. On the other hand, with the proposed controller, the quadrotor can still accurately track the desired trajectory even in the presence of both model uncertainties and step input disturbances. The experimental results have demonstrated the superior robustness of the developed control strategies over the existing quaternion-based robust controllers for handling model uncertainties and disturbances. The control inputs are shown in Fig. 15.

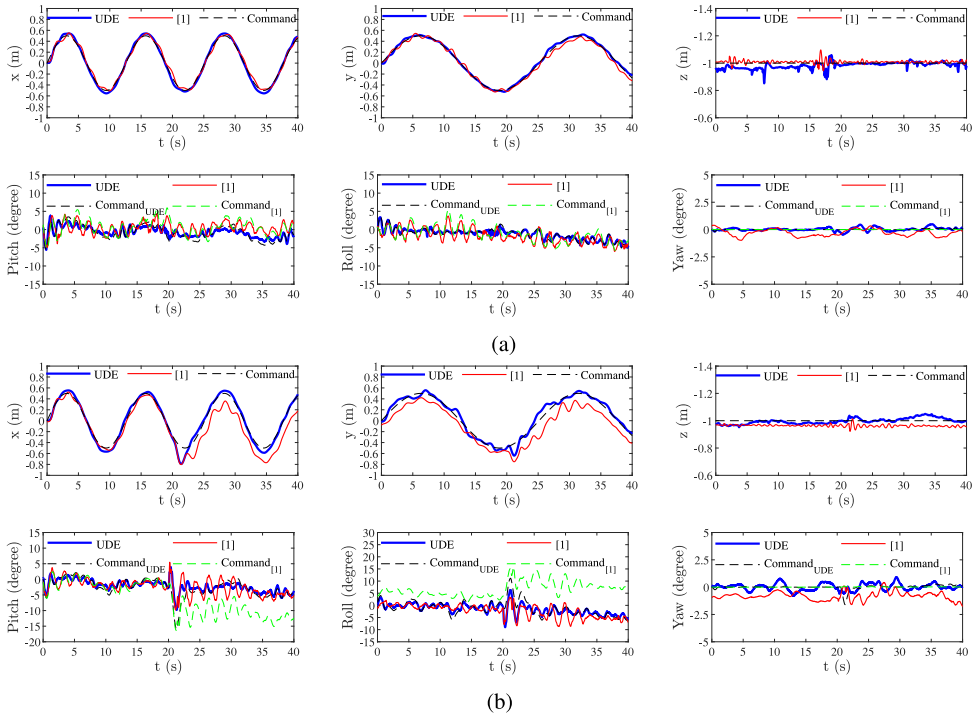

Fig. 14. Case III: Comparison with the existing robust controller: positions and Euler angles. (a) Nominal scenario without uncertainty and disturbance. (b) Uncertainty and disturbance rejection scenario with the uncertainty added at $t = 0$ s and disturbance added at $t = 20$ s.

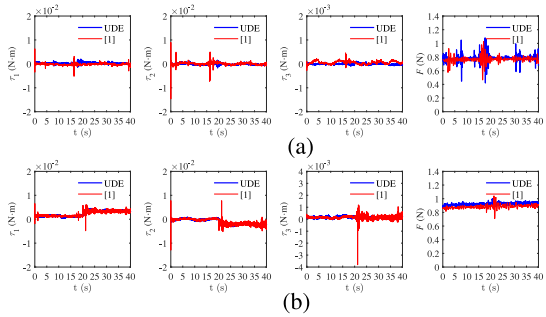

Fig. 15. Case III: Comparison with the existing robust controller: control inputs. (a) Nominal scenario. (b) Uncertainty and disturbance rejection scenario.

VI. Conclusion

In this article, the UDE-based attitude and position controllers with the unit quaternion formulation have been developed for a quadrotor to achieve the robust global singularity-free control in the presence of system coupling, model uncertainties, and external disturbances. A nonlinear unit quaternion-based reference model has been introduced to attain the time-scale separation between the position loop and attitude loop. The boundedness of attitude tracking errors were guaranteed via Lyapunov-based stability analysis. Extensive flight experiments were performed to demonstrate the capabilities of developed controllers for recovering from undesirable large initial angles, accurate trajectory tracking under the influence of external wind disturbance, and the superior robustness over the existing quaternion-based robust control algorithms.

Acknowledgment

The authors would like to thank the editors and the reviewers for their constructive suggestions and comments, which have greatly improved the quality of this article.

References

[1] R. Naldi, M. Furci, R. G. Sanfelice, and L. Marconi, "Robust global trajectory tracking for underactuated VTOL aerial vehicles using inner-outer loop control paradigms," *IEEE Trans. Autom. Control*, vol. 62, no. 1, pp. 97–112, Jan. 2017.

[2] E. Kayacan and R. Maslim, "Type-2 Fuzzy logic trajectory tracking control of quadrotor VTOL aircraft with elliptic membership functions," *IEEE/ASME Trans. Mechatron.*, vol. 22, no. 1, pp. 339–348, Feb. 2017.

[3] M. Faessler, A. Franchi, and D. Scaramuzza, "Differential flatness of quadrotor dynamics subject to rotor drag for accurate tracking of high-speed trajectories," *IEEE Robot. Autom. Lett.*, vol. 3, no. 2, pp. 620–626, Apr. 2018.

[4] D. Brescianini, M. Hehn, and R. D'Andrea, "Nonlinear quadrocopter attitude control," Department of Mechanical and Process Engineering, Swiss Federal Institute of Technology, Zurich, Switzerland, Tech. Rep. 009970340, 2013.

[5] J. Thomas *et al.*, "Aggressive flight with quadrotors for perching on inclined surfaces," *ASME J. Mechanisms Robot.*, vol. 8, no. 5, May 2016, Art. no. 051007.

[6] S. Sun, L. Sijbers, X. Wang, and C. de Visser, "High-speed flight of quadrotor despite loss of single rotor," *IEEE Robot. Autom. Lett.*, vol. 3, no. 4, pp. 3201–3207, Oct. 2018.

[7] S. Islam, P. Liu, and A. El Saddik, "Robust control of four-rotor unmanned aerial vehicle with disturbance uncertainty," *IEEE Trans. Ind. Electron.*, vol. 62, no. 3, pp. 1563–1571, Mar. 2015.

[8] T. Lee, "Robust adaptive attitude tracking on SO(3) with an application to a quadrotor UAV," *IEEE Trans. Control Syst. Technol.*, vol. 21, no. 5, pp. 1924–1930, Sep. 2013.

[9] Y. Yu and X. Ding, "A global tracking controller for underactuated aerial vehicles: Design, analysis, and experimental tests on quadrotor," *IEEE/ASME Trans. Mechatron.*, vol. 21, no. 5, pp. 2499–2511, Oct. 2016.

[10] R. Mahony, T. Hamel, and J. Pflimlin, "Nonlinear complementary filters on the special orthogonal group," *IEEE Trans. Autom. Control*, vol. 53, no. 5, pp. 1203–1218, Jun. 2008.
[11] J. Moreno-Valenzuela, R. Pérez-Alcocer, M. Guerrero-Medina, and A. Dzul, "Nonlinear PID-type controller for quadrotor trajectory tracking," *IEEE/ASME Trans. Mechatron.*, vol. 23, no. 5, pp. 2436–2447, Oct. 2018.
[12] B. Zhao, B. Xian, Y. Zhang, and X. Zhang, "Nonlinear robust adaptive tracking control of a quadrotor UAV via immersion and invariance methodology," *IEEE Trans. Ind. Electron.*, vol. 62, no. 5, pp. 2891–2902, May 2015.
[13] F. Chen, R. Jiang, K. Zhang, B. Jiang, and G. Tao, "Robust backstepping sliding-mode control and observer-based fault estimation for a quadrotor UAV," *IEEE Trans. Ind. Electron.*, vol. 63, no. 8, pp. 5044–5056, Aug. 2016.
[14] H. Liu, W. Zhao, Z. Zuo, and Y. Zhong, "Robust control for quadrotors with multiple time-varying uncertainties and delays," *IEEE Trans. Ind. Electron.*, vol. 64, no. 2, pp. 1303–1312, Feb. 2017.
[15] H. Yang, L. Cheng, Y. Xia, and Y. Yuan, "Active disturbance rejection attitude control for a dual closed-loop quadrotor under gust wind," *IEEE Trans. Control Syst. Technol.*, vol. 26, no. 4, pp. 1400–1405, Jul. 2018.
[16] A. Poultney, C. Kennedy, G. Clayton, and H. Ashrafiuon, "Robust tracking control of quadrotors based on differential flatness: Simulations and experiments," *IEEE/ASME Trans. Mechatron.*, vol. 23, no. 3, pp. 1126–1137, Jun. 2018.
[17] R. Sanz, P. Garcia, Q.-C. Zhong, and P. Albertos, "Robust control of quadrotors based on an uncertainty and disturbance estimator," *ASME Trans. J. Dyn. Syst. Meas. Control*, vol. 138, no. 7, 2016, Art. no. 071006.
[18] Q. Lu, B. Ren, S. Parameswaran, and Q.-C. Zhong, "Uncertainty and disturbance estimator-based robust trajectory tracking control for a quadrotor in a global positioning system-denied environment," *ASME Trans. J. Dyn. Syst. Meas. Control*, vol. 140, no. 3, Mar. 2017, Art. no. 031001.
[19] Q. Lu, B. Ren, and S. Parameswaran, "Shipboard landing control enabled by an uncertainty and disturbance estimator," *AIAA J. Guid., Control, Dyn.*, vol. 41, no. 7, pp. 1502–1520, Jul. 2018.
[20] N. A. Chaturvedi, A. K. Sanyal, and N. H. McClamroch, "Rigid-body attitude control," *IEEE Control Syst. Mag.*, vol. 31, no. 3, pp. 30–51, Jun. 2011.
[21] F. A. Goodarzi, D. Lee, and T. Lee, "Geometric adaptive tracking control of a quadrotor UAV on SE (3) for agile maneuvers," *ASME Trans. J. Dyn. Syst. Meas. Control*, vol. 137, no. 9, Jun. 2015, Art. no. 091007.
[22] X. Shi, Y. Zhang, and D. Zhou, "Almost-global finite-time trajectory tracking control for quadrotors in the exponential coordinates," *IEEE Trans. Aerosp. Electron. Syst.*, vol. 53, no. 1, pp. 91–100, Feb. 2017.
[23] D. S. Maithripala and J. M. Berg, "An intrinsic PID controller for mechanical systems on Lie groups," *Automatica*, vol. 54, pp. 189–200, Apr. 2015.
[24] A. Tayebi and S. McGilvray, "Attitude stabilization of a VTOL quadrotor aircraft," *IEEE Trans. Control Syst. Technol.*, vol. 14, no. 3, pp. 562–571, May 2006.
[25] M. Cutler and J. P. How, "Analysis and control of a variable-pitch quadrotor for agile flight," *ASME Trans. J. Dyn. Syst. Meas. Control*, vol. 137, no. 10, 2015, Art. no. 101002.
[26] H. Liu, X. Wang, and Y. Zhong, "Quaternion-based robust attitude control for uncertain robotic quadrotors," *IEEE Trans. Ind. Informat.*, vol. 11, no. 2, pp. 406–415, Apr. 2015.
[27] H. Liu, J. Xi, and Y. Zhong, "Robust attitude stabilization for nonlinear quadrotor systems with uncertainties and delays," *IEEE Trans. Ind. Electron.*, vol. 64, no. 7, pp. 5585–5594, Jul. 2017.
[28] A. Castillo, R. Sanz, P. Garcia, W. Qiu, H. Wang, and C. Xu, "Disturbance observer-based quadrotor attitude tracking control for aggressive maneuvers," *Control Eng. Pract.*, vol. 82, pp. 14–23, Jan. 2019.
[29] Y.-S. Zhong, "Robust output tracking control of SISO plants with multiple operating points and with parametric and unstructured uncertainties," *Int. J. Control*, vol. 75, no. 4, pp. 219–241, Nov. 2002.
[30] Q.-C. Zhong and D. Rees, "Control of uncertain LTI systems based on an uncertainty and disturbance estimator," *ASME Trans. J. Dyn. Syst. Meas. Control*, vol. 126, no. 4, pp. 905–910, Dec. 2004.
[31] B. Ren, Q.-C. Zhong, and J. Dai, "Asymptotic reference tracking and disturbance rejection of UDE-based robust control," *IEEE Trans. Ind. Electron.*, vol. 64, no. 4, pp. 3166–3176, Apr. 2017.
[32] K. Youcef-Toumi and O. Ito, "A time delay controller for systems with unknown dynamics," *ASME Trans. J. Dyn. Syst. Meas. Control*, vol. 112, no. 1, pp. 133–142, Mar. 1990.
[33] J. Dai, B. Ren, and Q.-C. Zhong, "Uncertainty and disturbance estimator-based backstepping control for nonlinear systems with mismatched uncertainties and disturbances," *ASME Trans. J. Dyn. Syst. Meas. Control*, vol. 140, no. 12, Dec. 2018, Art. no. 121005.
[34] A. Tayebi, "Unit quaternion-based output feedback for the attitude tracking problem," *IEEE Trans. Autom. Control*, vol. 53, no. 6, pp. 1516–1520, Jul. 2008.
[35] J. C. Chou, "Quaternion kinematic and dynamic differential equations," *IEEE Trans. Robot. Autom.*, vol. 8, no. 1, pp. 53–64, Feb. 1992.
[36] F. L. Markley, "Fast quaternion attitude estimation from two vector measurements," *AIAA J. Guid., Control, Dyn.*, vol. 25, no. 2, pp. 411–414, Mar. 2002.
[37] Y.-C. Choi and H.-S. Ahn, "Nonlinear control of quadrotor for point tracking: Actual implementation and experimental tests," *IEEE/ASME Trans. Mechatron.*, vol. 20, no. 3, pp. 1179–1192, Jun. 2015.
[38] PARROT Minidrones Support from Simulink, Sep. 10, 2018. [Online]. Available: https://ww2.mathworks.cn/hardware-support/parrot-minidrones.html
[39] M. Faessler, F. Fontana, C. Forster, and D. Scaramuzza, "Automatic re-initialization and failure recovery for aggressive flight with a monocular vision-based quadrotor," in *Proc. IEEE Int. Conf. Robot. Autom.*, 2015, pp. 1722–1729.

Qi Lu (Member, IEEE) received the B.Eng. degree in mechanical engineering from China Agricultural University, Beijing, China, in 2012, the M.Sc. degree in mechanical engineering from the University of Florida, Gainesville, FL, USA, in 2014 and the Ph.D. degree in mechanical engineering from Texas Tech University, Lubbock, TX, USA, in 2019.

Since 2019, he has been with the Department of Mechanical Engineering, Sichuan University-Pittsburgh Institute, Sichuan University, Chengdu, Sichuan, China, as an Assistant Professor. His current research interests include navigation and control of unmanned aerial vehicles, multiagent system and robotics.

Beibei Ren (Senior Member, IEEE) received the B.Eng. degree in mechanical and electronic engineering and the M.Eng. degree in automation from Xidian University, Xi'an, China, in 2001 and 2004, respectively, and the Ph.D. degree in the electrical and computer engineering from the National University of Singapore, Singapore, in 2010.

From 2010 to 2013, she was a Postdoctoral Scholar with the Department of Mechanical and Aerospace Engineering, University of California, San Diego, CA, USA. She is currently an Associate Professor with the Department of Mechanical Engineering, Texas Tech University, Lubbock, TX, USA. Her current research interests include robust control theory and its application to mechatronics, and renewable energy systems.

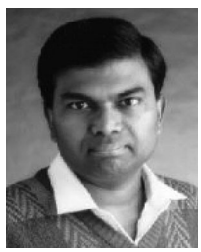

Siva Parameswaran received the M.Sc. (Distinction) and Ph.D. degrees in mechanical engineering from Imperial College London, London, U.K. in 1979 and 1986, respectively.

Since 1989, he has been with the Department of Mechanical Engineering, Texas Tech University, Lubbock, TX, USA, where he is currently a Professor. He is also a Guest Professor with Jiangsu University, Zhenjiang, China. His current research interests include jet impingement cooling, high frequency oscillating ventilators, and turbine–turbine interaction.

Dr. Parameswaran is a Fellow of ASME.